PAPER

Nonreciprocal Photon Blockade Based on Zeeman Splittings Induced by a Fictitious Magnetic Field

Nonreciprocal Photon Blockade Based on Zeeman Splittings Induced by a Fictitious Magnetic Field

Xin Su(苏欣)[1,2], Biao-Bing Jin(金飚兵)[2], Jiang-Shan Tang(唐江山)[1*], and Keyu Xia(夏可宇)[1*]

[1]*College of Engineering and Applied Sciences, National Laboratory of Solid State Microstructures, and Collaborative Innovation Center of Advanced Microstructures, Nanjing University, Nanjing 210023, China*
[2]*Research Institute of Superconductor Electronics (RISE) & Key Laboratory of Optoelectronic Devices and Systems with Extreme Performances of MOE, School of Electronic Science and Engineering, Nanjing University, Nanjing 210023, China*

(Received 16 April 2024; accepted manuscript online 7 June 2024)

Quantum nonreciprocity, such as nonreciprocal photon blockade, has attracted a great deal of attention due to its unique applications in quantum information processing. Its implementation primarily relies on rotating nonlinear systems, based on the Sagnac effect. Here, we propose an all-optical approach to achieve nonreciprocal photon blockade in an on-chip microring resonator coupled to a V-type Rb atom, which arises from the Zeeman splittings of the atomic hyperfine sublevels induced by the fictitious magnetic field of a circularly polarized control laser. The system manifests single-photon blockade or multi-photon tunneling when driven from opposite directions. This nonreciprocity results from the directional detunings between the countercirculating probe fields and the V-type atom, which does not require the mechanical rotation and facilitates integration. Our work opens up a new route to achieve on-chip integrable quantum nonreciprocity, enabling applications in chiral quantum technologies.

DOI: 10.1088/0256-307X/41/7/074202

Nonreciprocal optical devices, such as isolators, circulators, and unidirectional amplifiers, play a crucial role in optical communication and signal processing by safeguarding the signal source against noise. Optical nonreciprocity[1,2] is typically achieved in magneto-optics materials with the magnetic circular dichroism and circular birefringence.[3–5] To avoid challenge of integrating magnet-based nonreciprocal devices on a chip, alternative strategies to realize magnetic-free optical nonreciprocity have been experimentally demonstrated and theoretically proposed, such as optical nonlinearities,[6–15] spatiotemporal modulation of dielectric permittivity,[16–20] atomic gases with susceptibility-momentum locking,[21–24] optomechanical (OM) systems,[25–29] spinning resonators,[30–37] moving atomic lattices,[38–40] chiral light-matter interaction,[41–46] and light-induced magnetization of atomic media.[47,48] In addition to nonreciprocal transmission or amplification in the classical regime, nonreciprocal quantum devices with different critical functionalities, e.g., single-photon diodes,[21,23,45] nonreciprocal single-photon band,[49] one-way quantum amplifiers,[50–52] nonreciprocal entanglements,[37] and nonreciprocal photon blockades (PBs),[31–36,53] have been intensively explored. These schemes not only reveal new physics under quantum regime, but can also provide promising applications in unconventional quantum information processing and chiral quantum technologies.

In particular, PBs, as a purely quantum correlation effect, play a pivotal role in the precise manipulation of single photons for fundamental physics investigations and practical applications in quantum information processing. Conventional PBs are experimentally demonstrated and theoretically predicted in cavity-QED[54–59] and circuit-QED[60–63] systems, Rydberg atoms,[64,65] OM systems,[66–68] and nonlinear optical systems.[69–72] In addition, the conventional PBs can be switched on and off in nonlinear optical systems with exceptional points.[73,74] These phenomena unveil the single-photon nonlinearities arising from factors such as quantum coherence in the atoms (or artificial atoms) or radiation-pressure coupling.

Nonreciprocal PB has been predicted in spinning Kerr resonators,[31,36] a spinning resonator coupled to a two-level atom[32] or quadratic OM systems,[33] which is based on the conventional condition of strong single-photon nonlinearity. Moreover, nonreciprocal unconventional PB, which relies on destructive interferences of different pathways, has been proposed in spinning OM systems[34] and spinning resonators with parametric amplification.[35] Most protocols designed to achieve nonreciprocal PBs or nonreciprocal unconventional PBs typically involve the use of rotating nonlinear components. In contrast, we propose a light-controlled nonreciprocal PB system without the need of mechanical rotation.

In this Letter, we propose the realization of nonreciprocal PB in a microring resonator chirally coupled to a V-type ^{87}Rb atom. The V-type level structure arises from the vector Stark shifts of atomic hyperfine sublevels with

*Corresponding authors. Email: js.tang@nju.edu.cn; keyu.xia@nju.edu.cn

the form of Zeeman splitting, which are induced and controlled by a circularly polarized control laser. The probe light fields incident to opposite directions couple to the splitting σ^+ and σ^- transitions of the V-type atom with red and blue detunings, respectively. This directional detuning gives rise to directional energy-level structures of the resonator-atom coupling system. By this means we obtain the magnetic-free quantum nonreciprocity. Single-photon blockade (1PB) with the second-order correlation $g^{(2)}(0) \sim 0.2$ or multi-photon tunneling with $g^{(2)}(0) \sim 230$ can emerge when driving the resonator from its opposite sides. Our scheme circumvents the need for mechanical rotation, presenting a promising avenue for realizing quantum nonreciprocity in integrable quantum information processing.

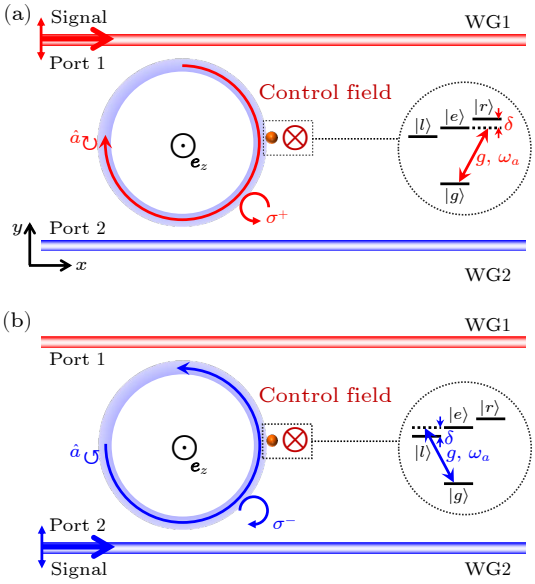

Fig. 1. Schematic of an all-optical nonreciprocal system consisting of a microring resonator (of resonance frequency ω_a) coupled to a ^{87}Rb atom and two nearby waveguides (WG1 and WG2). A LCP control field is applied along $-\boldsymbol{e}_z$ and generates a fictitious magnetic field (FMF) along $\boldsymbol{e}_z$, where $\boldsymbol{e}_z$ is the real-valued unit vector of z axis. The evanescent electric field of the CW mode is σ^+ polarized near the outer sidewall, while that for the CCW mode is σ^- polarized. (a) A signal input to WG1 from port 1 excites the CW mode $\hat{a}_\circlearrowleft$ which couples to the σ^+ transition $|g\rangle \leftrightarrow |r\rangle$ within the Rb atom's D_1 line. (b) A signal input to WG2 from port 2 excites the CCW mode $\hat{a}_\circlearrowleft$ which couples to the σ^- transition $|g\rangle \leftrightarrow |l\rangle$.

System. A schematic diagram of our setup is present in Fig. 1. The whispering-gallery mode (WGM) microring resonator, characterized by a resonance frequency ω_a and a damping rate κ, is coupled with a single ^{87}Rb atom. A circularly polarized control laser, with a frequency ω detuned between D_1 and D_2 lines of the Rb atom, can induce vector Stark shifts[75–78] exclusively in its hyperfine-structure (HFS) magnetic sublevels within a $J = 1/2$ fine-state manifold. The shifts are proportional to $m_{\rm F}$ and thus are called the Zeeman splitting induced by a fictitious magnetic field (FMF),[75,79] where $m_{\rm F}$ is the quantum number for the projection of atomic angular momentum onto the quantization axis. The HFS magnetic sublevels in the nJ manifold are also subject to a scalar Stark shift (the same for all states in the nJ manifold) and tensor Stark shifts proportional to $m_{\rm F}^2$.[75–78] Nevertheless, the scalar Stark shift can be eliminated with proper tuning of the control field and the tensor Stark shifts vanish for $J = 1/2$ manifolds (see Supplementary Material). A properly detuned left-circularly polarized (LCP) control laser is applied along negative z axis, generating an FMF directed to z axis.

The signal from port 1 or port 2 is almost exclusively transversally polarized along y axis, whereas the evanescent electric field circulating around the sidewalls of the resonator has a local longitudinal component besides the radial component due to the strong transverse confinement.[46,80,81] These two components are $\pm\pi/2$ out of phase with each other, with the $\pm$ sign depending on propagating directions of WGMs. The sidewall evanescent fields can be nearly perfectly circularly polarized for a high-refractive-index WGM resonator. Assuming $\boldsymbol{e}_z$ as the quantization axis (see Fig. 1), the evanescent electric field of the clockwise (CW) mode is σ^+ polarized near the outer sidewall, while that for the counterclockwise (CCW) mode is σ^- polarized. The 795-nm-band CW and CCW modes $\hat{a}_\circlearrowleft$ and $\hat{a}_\circlearrowleft$ are resonant with the D_1-line π transition $|5S_{1/2}, F = 1, m_{\rm F} = 0\rangle \leftrightarrow |5P_{1/2}, F' = 2, m_{\rm F'} = 0\rangle$, where only the $5P_{1/2}$-manifold scalar Stark shift does not vanish but can be ignored for its magnitude of tens of megahertz. The mode $\hat{a}_\circlearrowleft$ ($\hat{a}_\circlearrowleft$) is red (blue) detuned to and couples to the σ^+ (σ^-) transition $|F = 1, m_{\rm F} = 0\rangle \leftrightarrow |F' = 2, m_{\rm F'} = +1\rangle$ ($|F' = 2, m_{\rm F'} = -1\rangle$) within the perturbatively shifted D_1 line. The vector Stark shifts of relevant states $|5P_{1/2}, F' = 2, m_{\rm F'} = \pm 1\rangle$ are $\pm\delta$ of tens of megahertz. For convenience, the ground state $|5S_{1/2}, F = 1, m_{\rm F} = 0\rangle$ is denoted as $|g\rangle$, the excited Zeeman sublevels $|5P_{1/2}, F' = 2, m_{\rm F'} = 0, \pm 1\rangle$ are denoted as $|e\rangle$, $|r\rangle$, and $|l\rangle$, respectively. The σ^+ and σ^- transitions, detuned in the blue or red shifts relative to the degenerate countercirculating modes by $\pm\delta$, induce different nonlinear energy-level structures of the system depending on light circulating direction.

The classical and quantum nonreciprocity, facilitated by chiral light-atom interactions, is typically achieved through two distinct mechanisms: the directional detunings between light and atomic transitions[46] and the unbalanced light-atom coupling strengths.[42,45] In order to achieve the photon blockade and photon tunneling in opposite directions through the unbalanced light-atom coupling, it is necessary for the coupling strengths to follow the specific condition $g_- = \sqrt{2}g_+$ (or $g_+ = \sqrt{2}g_-$). Here g_+ (g_-) is the coupling strength between the σ^+ (σ^-) atomic transition and the σ^+- (σ^--) polarized field. However, it is hard to find such a pair of σ^+ and σ^- transitions in a natural atom whose light-atom coupling strengths satisfy the above condition. As a contrast, the magnitude of the directional detuning δ can be adjusted arbitrarily by controlling the control field intensity to achieve the nonreciprocal photon blockade. Therefore, compared to the

unbalanced light-atom coupling, the scheme of directional detunings is more feasible in experiments.

Zeeman Splitting of Rubidium 87 D_1 Line. When an atom in the state $|\psi_0\rangle$ is irradiated by a laser field with an oscillating electric field $\boldsymbol{E}(t) = \mathcal{E}\boldsymbol{\epsilon}e^{-i\omega t} + \mathcal{E}^*\boldsymbol{\epsilon}^* e^{i\omega t}$ far from resonance with the atom ($\boldsymbol{\epsilon}$ is the complex unit vector of the polarization), the second-order ac Stark shift of the atomic state $|\psi_0\rangle$ is

$$U_{\rm AC}(\psi_0) = \frac{|\mathcal{E}|^2}{\hbar}\sum_{n\neq 0}{\rm Re}\Big[\frac{\langle\psi_0|\hat{\boldsymbol{d}}\cdot\boldsymbol{\epsilon}^*|\psi_n\rangle\langle\psi_n|\hat{\boldsymbol{d}}\cdot\boldsymbol{\epsilon}|\psi_0\rangle}{\omega-(\omega_n-\omega_0)+i\gamma_{n0}/2} - \frac{\langle\psi_0|\hat{\boldsymbol{d}}\cdot\boldsymbol{\epsilon}|\psi_n\rangle\langle\psi_n|\hat{\boldsymbol{d}}\cdot\boldsymbol{\epsilon}^*|\psi_0\rangle}{\omega+(\omega_n-\omega_0)+i\gamma_{n0}/2}\Big], \quad (1)$$

where $|\psi_0\rangle$ and $|\psi_n\rangle$ are the initial state and all possible final states of the atom, with unperturbed energies $\hbar\omega_0$ and $\hbar\omega_n$, respectively; $\gamma_{n0} = \gamma_n + \gamma_0$ is the transition linewidth with γ_0 and γ_n being spontaneous decay rates of states $|\psi_0\rangle$ and $|\psi_n\rangle$; and $\hat{\boldsymbol{d}}$ is the operator for the electric dipole of the atom.

After the calculation in the formalism of irreducible tensor operator, the ac Stark shift of the ground-state hyperfine sublevel $|nS_{1/2},\, F,\, m_{\rm F}\rangle$ of the alkali atom, as shown in the Supplementary Material, can be written as

$$U_{\rm AC}(nS_{1/2},\, F,\, m_{\rm F}) = -i\beta_{nS_{1/2}}g_{\rm F}\langle F, m_{\rm F}|\hat{\boldsymbol{\sigma}}|F, m_{\rm F}\rangle \cdot(\boldsymbol{\mathcal{E}}\times\boldsymbol{\mathcal{E}}^*) + \alpha_{nS_{1/2}}|\boldsymbol{\mathcal{E}}|^2, \quad (2)$$

where $\alpha_{nS_{1/2}}$ and $\beta_{nS_{1/2}}$ are the scalar and the vector polarizabilities for the $nS_{1/2}$ manifold, respectively; $g_{\rm F}$ is the Landé factor for the hyperfine state $|nS_{1/2},\, F\rangle$, and $\hat{\boldsymbol{\sigma}}$ is the Pauli spin operator. The first term in Eq. (2) plays the role of an effective Zeeman splitting. We have

$$\begin{aligned}\alpha_{nS_{1/2}} = {}& \frac{1}{6\hbar}|\langle nS_{1/2}\|\hat{\boldsymbol{d}}\|nP_{1/2}\rangle|^2 \\ & \times{\rm Re}\Big(\frac{1}{\omega-\omega_{D_1}+i\gamma_{D_1}} - \frac{1}{\omega+\omega_{D_1}+i\gamma_{D_1}}\Big) \\ & + \frac{1}{6\hbar}|\langle nS_{1/2}\|\hat{\boldsymbol{d}}\|nP_{3/2}\rangle|^2 \\ & \times{\rm Re}\Big(\frac{1}{\omega-\omega_{D_2}+i\gamma_{D_2}} - \frac{1}{\omega+\omega_{D_2}+i\gamma_{D_2}}\Big), \end{aligned} \quad (3)$$

$$\begin{aligned}\beta_{nS_{1/2}} = {}& \frac{2}{6g_{nS_{1/2}}\hbar}|\langle nS_{1/2}\|\hat{\boldsymbol{d}}\|nP_{1/2}\rangle|^2 \\ & \times{\rm Re}\Big(\frac{1}{\omega-\omega_{D_1}+i\gamma_{D_1}} + \frac{1}{\omega+\omega_{D_1}+i\gamma_{D_1}}\Big) \\ & - \frac{1}{6g_{nS_{1/2}}\hbar}|\langle nS_{1/2}\|\hat{\boldsymbol{d}}\|nP_{3/2}\rangle|^2 \\ & \times{\rm Re}\Big(\frac{1}{\omega-\omega_{D_2}+i\gamma_{D_2}} + \frac{1}{\omega+\omega_{D_2}+i\gamma_{D_2}}\Big), \end{aligned} \quad (4)$$

where $\omega_{D_1} = \omega_{nP_{1/2}} - \omega_{nS_{1/2}}$, $\omega_{D_2} = \omega_{nP_{3/2}} - \omega_{nS_{1/2}}$; γ_{D_1} (γ_{D_2}) is the decay rate of the $|nS_{1/2}\rangle \leftrightarrow |nP_{1/2}\rangle$ ($|nP_{3/2}\rangle$) transition; and $g_{nS_{1/2}}$ is the Landé factor for the fine-structure ground state $|nS_{1/2}\rangle$. Here we neglect couplings other than D_1 and D_2.

The ac Stark shift in Eq. (2) can be rewritten in a form of the scalar Stark shift plus the Zeeman shift,

$$U(nS_{1/2},\, F,\, m_{\rm F}) = \alpha_{nS_{1/2}}|\mathcal{E}|^2 + \eta\beta_{nS_{1/2}}|\mathcal{E}|^2 g_{\rm F} m_{\rm F}, \quad (5)$$

where $\eta = -i\boldsymbol{e}_k\cdot(\boldsymbol{\epsilon}\times\boldsymbol{\epsilon}^*)$ is the degree of circularity. Here, $\boldsymbol{e}_k$, the direction of light propagation, is the quantization axis that defines $m_{\rm F}$. The second term in Eq. (5) has the same form as a Zeeman shift, $g_{\rm F}m_{\rm F}\mu_{\rm B}B_{\rm fic}$, of an atom in the $|nS_{1/2},\, F,\, m_{\rm F}\rangle$ state inside a magnetic field $B_{\rm fic}\boldsymbol{e}_k$, where $\mu_{\rm B}$ is the Bohr magneton. Here we define the light-induced FMF as

$$B_{\rm fic} = \frac{\eta\beta_{nS_{1/2}}|\mathcal{E}|^2}{\mu_{\rm B}}, \quad (6)$$

with $B_{\rm fic}$ the same for all HFS sublevels $|nJFm_{\rm F}\rangle$ within an nJ manifold. The direction of $B_{\rm fic}$ is determined by the polarization of the light, as $\eta = +1$ for a right-circularly polarized (RCP) light, and $\eta = -1$ for an LCP light. $B_{\rm fic}$ vanishes for a linearly polarized light as $\eta = 0$ in this case.

When the control laser is tuned between the alkali-metal D transitions, the spontaneous decay rates of D_1 and D_2 transitions and farther off-resonance terms in Eqs. (3) and (4) are neglected. Considering ac Stark shifts of the D_1-line states of ^{87}Rb atom, the scalar and vector polarizabilities for all HFS sublevels $|5S_{1/2},\, F,\, m_{\rm F}\rangle$ within the $5S_{1/2}$ manifold take the approximate forms

$$\begin{aligned}\alpha_{5S_{1/2}} &\simeq \frac{|\langle 5S_{1/2}\|\hat{\boldsymbol{d}}\|5P_{1/2}\rangle|^2}{6\hbar}\Big[\frac{1}{\Delta_{D_1}} + \frac{2}{\Delta_{D_2}}\Big], \\ \beta_{5S_{1/2}} &\simeq \frac{|\langle 5S_{1/2}\|\hat{\boldsymbol{d}}\|5P_{1/2}\rangle|^2}{6\hbar}\Big[\frac{1}{\Delta_{D_1}} - \frac{1}{\Delta_{D_2}}\Big], \end{aligned} \quad (7)$$

where $\Delta_{D_1} = \omega - \omega_{D_1}$, $\Delta_{D_2} = \omega - \omega_{D_2}$. We use $g_{5S_{1/2}} = 2$ and $|\langle 5S_{1/2}\|\hat{\boldsymbol{d}}\|5P_{3/2}\rangle|^2 \approx 2|\langle 5S_{1/2}\|\hat{\boldsymbol{d}}\|5P_{1/2}\rangle|^2$. It is obvious from Eq. (7) that the scalar Stark shift vanishes and only the vector Stark shifts remain when $\Delta_{D_2} = -2\Delta_{D_1}$. Under this condition, the ac Stark shifts of all HFS sublevels $|5S_{1/2},\, F,\, m_{\rm F}\rangle$ take the form of a pure Zeeman shift. Similarly, the scalar and vector polarizabilities for all HFS sublevels $|5P_{1/2},\, F',\, m_{\rm F'}\rangle$ within the $5P_{1/2}$ manifold take the approximate forms

$$\begin{aligned}\alpha_{5P_{1/2}} &\simeq -\frac{|\langle 5S_{1/2}\|\hat{\boldsymbol{d}}\|5P_{1/2}\rangle|^2}{6\hbar}\frac{1}{\Delta_{D_1}}, \\ \beta_{5P_{1/2}} &\simeq \frac{|\langle 5S_{1/2}\|\hat{\boldsymbol{d}}\|5P_{1/2}\rangle|^2}{2\hbar}\frac{1}{\Delta_{D_1}}, \end{aligned} \quad (8)$$

where $g_{5P_{1/2}} = 2/3$ is used.

In brief, under an RCP (LCP) control laser properly tuned between the alkali-metal D transitions, the hyperfine sublevels within ^{87}Rb D_1 line experience ac Stark shifts with the form of Zeeman splitting under the FMF along (against) the laser propagation direction.

Hamiltonian and Master Equation. The Hamiltonian of the system consisting of the countercirculating modes coupled to a Rb atom and the probe fields from WG1 and WG2, in the rotating frame, reads

$$\begin{aligned}\hat{H} &= \hat{H}_{\circlearrowleft} + \hat{H}_{\circlearrowright} + \hat{H}_{d,1} + \hat{H}_{d,2}, \\ \hat{H}_{\circlearrowleft} &= (\delta-\Delta)\hat{\sigma}_{rr} - \Delta\hat{a}^\dagger_{\circlearrowleft}\hat{a}_{\circlearrowleft} + g(\hat{a}^\dagger_{\circlearrowleft}\hat{\sigma}_{\rm gr} + \hat{\sigma}_{\rm rg}\hat{a}_{\circlearrowleft}), \\ \hat{H}_{\circlearrowright} &= (-\delta-\Delta)\hat{\sigma}_{ll} - \Delta\hat{a}^\dagger_{\circlearrowright}\hat{a}_{\circlearrowright} + g(\hat{a}^\dagger_{\circlearrowright}\hat{\sigma}_{\rm gl} + \hat{\sigma}_{\rm lg}\hat{a}_{\circlearrowright}), \\ \hat{H}_{d,1} &= -i\sqrt{\kappa_{\rm ex,1}}\alpha_{\rm in,1}(\hat{a}^\dagger_{\circlearrowleft} - \hat{a}_{\circlearrowleft}), \\ \hat{H}_{d,2} &= -i\sqrt{\kappa_{\rm ex,2}}\alpha_{\rm in,2}(\hat{a}^\dagger_{\circlearrowright} - \hat{a}_{\circlearrowright}), \end{aligned} \quad (9)$$

where $\Delta = \omega_{\rm p} - \omega_a$ and $\delta = \omega_{\rm rg} - \omega_0 = \omega_0 - \omega_{\rm lg}$ with ω_0 ($\omega_{\rm rg}$, $\omega_{\rm lg}$) denoting the resonance frequency of the π ($\sigma^{\pm}$) transition $|g\rangle \leftrightarrow |e\rangle$ ($|g\rangle \leftrightarrow |r, l\rangle$). Here the condition that the degenerate cavity modes are resonant with the π transition $|g\rangle \leftrightarrow |e\rangle$ is used, i.e., $\omega_a = \omega_0$; $\alpha_{\rm in,\,1}$ ($\alpha_{\rm in,\,2}$) is the amplitude of the probe field input to WG1 (WG2) from port 1 (2) which is normalized to a photon flux; $\kappa_{\rm ex,\,1}$ ($\kappa_{\rm ex,\,2}$) is the external decay rate of the CW mode or the CCW mode at the WG1-resonator (WG2-resonator) interface. The total system is divided into two uncoupled subsystems. The CW (CCW) mode couples to the σ^+ (σ^-) atomic transition at the rate g, which comprises the subsystem denoted by $\hat{H}_{\circlearrowright}$ ($\hat{H}_{\circlearrowleft}$) and gives the anharmonic energy-level structure of the subsystem. By driving the system from its upper (lower) side, the subsystem denoted by $\hat{H}_{\circlearrowright}$ ($\hat{H}_{\circlearrowleft}$) is excited.

The master equation of the system takes the form

$$\begin{aligned}\dot{\rho} = & -i[\hat{H},\,\rho] + \mathscr{L}[\hat{L}_{\circlearrowright}]\rho + \mathscr{L}[\hat{L}_{\circlearrowleft}]\rho \\ & + \mathscr{L}[\hat{L}_{\sigma^+}]\rho + \mathscr{L}[\hat{L}_{\sigma^-}]\rho, \end{aligned} \tag{10}$$

where $\mathscr{L}[\hat{o}]\rho = \hat{o}\rho\hat{o}^{\dagger} - (\hat{o}^{\dagger}\hat{o}\rho + \rho\hat{o}^{\dagger}\hat{o})/2$ and ρ is the system density matrix. The term $\mathscr{L}[\hat{L}_{\circlearrowright}]$ ($\mathscr{L}[\hat{L}_{\circlearrowleft}]$) with the operator $\hat{L}_{\circlearrowright} = \sqrt{\kappa}\hat{a}_{\circlearrowright}$ ($\hat{L}_{\circlearrowleft} = \sqrt{\kappa}\hat{a}_{\circlearrowleft}$) describes the decay of the CW (CCW) mode with the rate κ. Here, $\kappa = \kappa_{\rm ex,\,1} + \kappa_{\rm ex,\,2}$. The term $\mathscr{L}[\hat{L}_{\sigma^+}]$ ($\mathscr{L}[\hat{L}_{\sigma^-}]$) with the operator $\hat{L}_{\sigma^+} = \sqrt{\gamma}\hat{\sigma}_{\rm gr}$ ($\hat{L}_{\sigma^-} = \sqrt{\gamma}\hat{\sigma}_{\rm gl}$) describes the spontaneous emission of the state $|r\rangle$ ($|l\rangle$) with the rate γ.

Directional Eigenspectra and Mechanism of Nonreciprocal Photon Blockade. Based on the FMF-induced Zeeman splitting of the atom, the directional detunings of the countercirculating resonator modes to the coupled σ^+ and σ^- atomic transitions ($\mp\delta$) are the origin of the nonreciprocal PB. When the coupling rate g satisfies certain relationship with δ, the one-photon resonance emerges when driving from the upper side and the two-photon resonance emerges when driving from the lower side with the same driving frequency. To give this relationship between g and δ, the directional eigenspectra of the system driven from either sides are solved (see the Supplementary Material). In the subsystem driven from the upper (lower) side which is described by $\hat{H}_{\circlearrowright}$ ($\hat{H}_{\circlearrowleft}$), the eigenvalues in the one- and two-photon excitation subspaces are solved as

$$\begin{aligned} E_{\circlearrowright}^{(1),\pm} &= \omega_a + \frac{\delta}{2} \pm \sqrt{\frac{\delta^2}{4} + g^2}, \\ E_{\circlearrowright}^{(2),\pm} &= 2\omega_a + \frac{\delta}{2} \pm \sqrt{\frac{\delta^2}{4} + 2g^2}, \\ E_{\circlearrowleft}^{(1),\pm} &= \omega_a - \frac{\delta}{2} \pm \sqrt{\frac{\delta^2}{4} + g^2}, \\ E_{\circlearrowleft}^{(2),\pm} &= 2\omega_a - \frac{\delta}{2} \pm \sqrt{\frac{\delta^2}{4} + 2g^2}. \end{aligned} \tag{11}$$

When the probe frequency $\omega_{\rm p}$ equals the eigenvalues $E_{\circlearrowright}^{(1),\,\pm}$ (one half of $E_{\circlearrowright}^{(2),\,\pm}$), the system is driven from its upper side with the single- (two-) photon resonant excitation. Thus, the probe detuning Δ with respect to the cavity resonance frequency in the one- (two-) photon resonant transition processes driven from the upper side is

$$\begin{aligned} \Delta &= \Delta_{\circlearrowright}^{(1),\pm} \equiv \frac{\delta}{2} \pm \sqrt{\frac{\delta^2}{4} + g^2}, \\ \Delta &= \Delta_{\circlearrowright}^{(2),\pm} \equiv \frac{\delta}{4} \pm \sqrt{\frac{\delta^2}{16} + \frac{g^2}{2}}. \end{aligned} \tag{12}$$

The probe detunings in the one- (two-) photon resonant transition processes driven from the lower side $\Delta_{\circlearrowleft}^{(1),\,\pm}$ ($\Delta_{\circlearrowleft}^{(2),\,\pm}$) are similarly obtained.

To observe the nonreciprocal PB under the same probe field frequency, the probe detuning Δ should satisfy the one- and two-photon resonance conditions, respectively, when driving from opposite sides. Concretely, we suppose that the one-photon resonance excitation is achieved when driving from the upper side, e.g., $\Delta = \Delta_{\circlearrowright}^{(1),\,-} \equiv \frac{\delta}{2} - \sqrt{\frac{\delta^2}{4} + g^2}$. As a contrast, it is assumed that a two-photon resonant transition is achieved when driving from the lower side, e.g., $\Delta = \Delta_{\circlearrowleft}^{(2),\,-} \equiv -\frac{\delta}{4} - \sqrt{\frac{\delta^2}{16} + \frac{g^2}{2}}$. The corresponding coupling rate g and the probe detuning Δ are solved as

$$g = \sqrt{6}\delta, \quad \Delta = -2\delta. \tag{13}$$

To visually understand the physical origin behind the nonreciprocal PB, the directional anharmonic energy-level diagrams of the system driven from opposite sides are shown in Fig. 2. The energy gaps in the one-photon excitation subspace are calculated by

$$\begin{aligned} \eta_1 &\equiv \omega_a - E_{\circlearrowright}^{(1),-} \equiv E_{\circlearrowleft}^{(1),+} - \omega_a = \sqrt{\frac{\delta^2}{4} + g^2} - \frac{\delta}{2}, \\ \eta_2 &\equiv E_{\circlearrowleft}^{(1),+} - \omega_a \equiv \omega_a - E_{\circlearrowright}^{(1),-} = \sqrt{\frac{\delta^2}{4} + g^2} + \frac{\delta}{2}. \end{aligned} \tag{14}$$

The energy gaps in the two-photon excitation subspace are

$$\begin{aligned} \eta_3 &\equiv 2\omega_a - E_{\circlearrowright}^{(2),-} \equiv E_{\circlearrowleft}^{(2),+} - 2\omega_a = \sqrt{\frac{\delta^2}{4} + 2g^2} - \frac{\delta}{2}, \\ \eta_4 &\equiv E_{\circlearrowleft}^{(2),+} - 2\omega_a \equiv 2\omega_a - E_{\circlearrowright}^{(2),-} = \sqrt{\frac{\delta^2}{4} + 2g^2} + \frac{\delta}{2}, \\ \eta_5 &\equiv E_{\circlearrowleft}^{(2),-} - 2E_{\circlearrowleft}^{(1),-}, \\ \eta_6 &\equiv \frac{1}{2}E_{\circlearrowleft}^{(2),-} - E_{\circlearrowleft}^{(1),-}. \end{aligned} \tag{15}$$

For the coupling rate $g = \sqrt{6}\delta$, which enables the one-photon resonance driven from the upper side to equal the two-photon resonance driven from the lower side, the energy gaps in Eqs. (14) and (15) become

$$\begin{aligned} &\eta_4 = 2\eta_1 = 4\delta, \quad \eta_2 = \eta_3 = 3\delta, \\ &\eta_5 = \delta = \eta_4 - \eta_3, \quad \eta_6 = \delta = \eta_2 - \eta_1. \end{aligned} \tag{16}$$

On the one hand, when the probe field with detuning $\Delta = -2\delta$ drives the system from its upper side, a single photon resonantly couples to the transition $|\psi^{(0)}\rangle \rightarrow |\psi_{\circlearrowright}^{(1),-}\rangle$. The following transition $|\psi_{\circlearrowright}^{(1),-}\rangle \rightarrow |\psi_{\circlearrowright}^{(2),-}\rangle$ is detuned by $\eta_5 = \delta$ to the successive single-photon excitations and thus is suppressed, as shown in Fig. 2. Once the system absorbs a first photon to be excited to $|\psi_{\circlearrowright}^{(1),-}\rangle$ state, the absorption of second one is blocked for its disability to resonantly excite the system to $|\psi_{\circlearrowright}^{(2),-}\rangle$

state, until the first photon is released out of the system from $|\psi_{\circlearrowleft}^{(1),-}\rangle$ state. Thus 1PB occurs for the CW optical mode. On the other hand, when the system is driven by the signal with detuning $\Delta = -2\delta$ from its lower side, two-photons resonantly excites the transition $|\psi^{(0)}\rangle \to |\psi_{\circlearrowleft}^{(2),-}\rangle$; whereas the transition $|\psi^{(0)}\rangle \to |\psi_{\circlearrowleft}^{(1),-}\rangle$ is detuned by $-\delta$ to the single photons and thus is suppressed, as shown in Fig. 2. The absorption of the first photon also favors that of the second or subsequent photons, i.e., resulting in photon-induced tunneling (PIT).[31] In this way, the unidirectional 1PB effect, in which 1PB emerges by driving from the upper side and PIT emerges by driving from the lower side under the same driving frequency, is realized with the V-type atom in which the σ^+ and σ^- transitions are blue and red detuned to the degenerate modes, respectively.

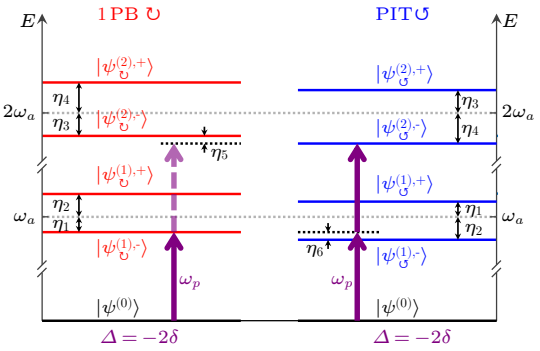

Fig. 2. Energy-level diagrams of the system driven from its upper or lower sides, with $\psi_{\circlearrowleft}^{(k)}$ ($\psi_{\circlearrowleft}^{(k)}$) denoting the k-photon resonant eigenstates of the subsystem driven along the CW (CCW) direction. Here, 1PB emerges by driving the device from its upper side, while two-photon tunneling occurs by driving from the lower side.

The vector Stark shifts of excited states $|r\rangle/|l\rangle$ are $\pm\delta = \pm g_{\rm F}\mu_{\rm B}B_{\rm fic}/\hbar$, respectively, with the FMF $B_{\rm fic} = \beta_{5P_{1/2}}|\mathcal{E}|^2/\mu_{\rm B}$. The electric field amplitude of the control laser is $\mathcal{E} = \sqrt{c\mu_0 I/2}$, where μ_0 is the vacuum permeability and I is the laser intensity. We take $I = 13\times10^8\ {\rm W/m^2}$, corresponding to $\mathcal{E} = 4.9485\times10^5\ {\rm V/m}$, $B_{\rm fic} = 54\,{\rm G}$, and $\delta/2\pi = 12.6\,{\rm MHz}$. The matched atomic coupling rate is $g = \sqrt{6}\delta = 2\pi\times30.88\,{\rm MHz}$, and the probe detuning is $\Delta/2\pi = -25.2\,{\rm MHz}$.

Results and Discussion. In what follows, we give the steady-state numerical results of the master equation (10) to recognize the nonreciprocal PB effect. The equal-time second- and higher-order correlation functions are introduced for opposite driving directions, i.e., $g_x^{(\mu)}(0) \equiv \langle\hat{a}_x^{\dagger\mu}\hat{a}_x^{\mu}\rangle/\langle\hat{a}_x^{\dagger}\hat{a}_x\rangle^{\mu}$ ($\mu \geqslant 2$), with $\mu = 2$ for recognizing the 1PB and $\mu > 2$ for distinguishing between multi-PB and the particular PIT. The subscript x can be ↻ (↺) to denote the case that the CW (CCW) mode is driven by the input from the resonator's upper (lower) side. The condition $g_x^{(\mu)}(0) > 1$ ($g_x^{(\mu)}(0) < 1$) indicates the μ-photon bunching (μ-photon antibunching). Hence $g_x^{(2)}(0) < 1$ characterizes 1PB via two-photon antibunching. To distinguish between multi-PB and the particular PIT, for example, two-photon blockade (2PB) and two-photon tunneling, 2PB characterized by three-photon antibunching and two-photon bunching must satisfy the following conditions with $\mu = 2$:[31]

$$g_x^{(\mu+1)}(0) < \exp(-\langle\hat{n}_x\rangle) \equiv f_x, \tag{17a}$$

$$g_x^{(\mu)}(0) \geq [\exp(-\langle\hat{n}_x\rangle) + \langle\hat{n}_x\rangle \cdot g_x^{(\mu+1)}(0)] \equiv f_x^{(\mu)}, \tag{17b}$$

where $\hat{n}_x \equiv \hat{a}_x^{\dagger}\hat{a}_x$. PIT is recognized by the following condition[31] simplified for $\langle\hat{n}_x\rangle \ll 1$:

$$g_x^{(\mu)}(0) > 1 \quad \text{for} \quad \mu = 2, 3, 4. \tag{18}$$

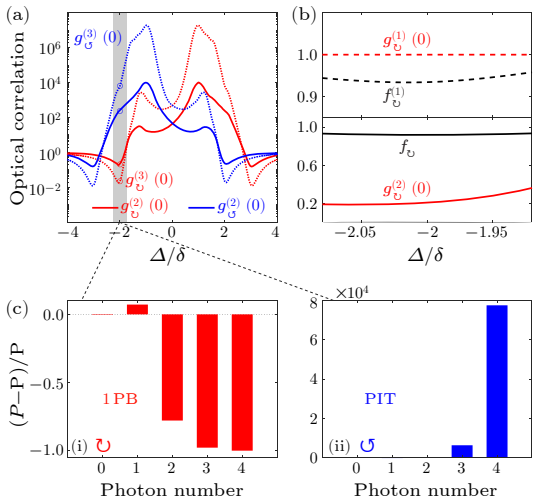

Fig. 3. (a) The equal-time second- and third-order correlation functions $g_x^{(2)}(0)$ (solid curves) and $g_x^{(3)}(0)$ (dotted curves) versus the optical detuning Δ for different driving directions. The subscript x is ↻ (↺) for the case of driving the CW (CCW) mode from the upper (lower) side. (b) Single-photon blockade (1PB) emerges at $\Delta = -2\delta$ by driving the resonator from its upper side, since $g_{\circlearrowleft}^{(2)}(0) < f_{\circlearrowleft}$ and $g_{\circlearrowleft}^{(1)}(0) > f_{\circlearrowleft}^{(1)}$ fulfill the criteria in Eq. (17) with $\mu = 1$. The directional PB effect can also be recognized from (c) the deviation of the intracavity photon-number distribution $P(n)$ from the Poisson distribution $\mathcal{P}(n)$ with the same mean photon number.

By driving the system from its upper side, $g_{\circlearrowleft}^{(3)}(0) \ll g_{\circlearrowleft}^{(2)}(0) \leqslant 0.2$ around the CW one-photon resonance $\Delta = \Delta_{\circlearrowleft}^{(1),-} = -2\delta$, as shown in Fig. 3(a). Thus it is indicated that 1PB emerges when driving from the upper side with the strong two- and three-photon antibunching of the CW mode. Concretely, $g_{\circlearrowleft}^{(2)}(0) \sim 0.2$ and $g_{\circlearrowleft}^{(3)}(0) \sim 0.02$. However, two-photon tunneling emerges around the same driving frequency when the device is driven from its lower side, with the frequency satisfying the two-photon resonance in the CCW direction, i.e., $\Delta = -2\delta = \Delta_{\circlearrowleft}^{(2),-}$. Figure 3(a) shows that $g_{\circlearrowleft}^{(3)}(0) \gg g_{\circlearrowleft}^{(2)}(0) \gg 1$ around $\Delta = -2\delta$, which satisfies the conditions given in Eq. (18). Specifically, $g_{\circlearrowleft}^{(3)}(0) \sim 6400$ and $g_{\circlearrowleft}^{(2)}(0) \sim 230$. Although $g_{\circlearrowleft}^{(2)}(0)$ shows a bunching effect, $g_{\circlearrowleft}^{(3)}(0) \gg g_{\circlearrowleft}^{(2)}(0)$ violates the criteria of the 2PB given by Eq. (17), which indicates the two-photon tunneling rather than the 2PB. In Fig. 3(b), $g_{\circlearrowleft}^{(1)}(0) \geq f_{\circlearrowleft}^{(1)} > f_{\circlearrowleft} > g_{\circlearrowleft}^{(2)}(0)$ around $\Delta = -2\delta$. Hence 1PB is confirmed by the criteria Eq. (17) with $\mu = 1$ and x being ↻. The difference of $g^{(2)}(0)$ for opposite directions can reach 3 orders of magnitude, suggesting a strongly nonreciprocal quantum statistics and quantum correlations.

The 1PB, multi-PB and PIT can also be recognized by the deviation of the photon-number distribution $P(n)$ in the resonator from the Poisson distribution $\mathcal{P}(n)$ with the same mean photon number, as shown in Fig. 3(c). The intracavity photon-number distribution is evaluated as

$$\begin{aligned} P(n) &= |\langle n, g|\varphi\rangle|^2 + |\langle n, r(l)|\varphi\rangle|^2 \\ &= \mathrm{Tr}[\rho(|n,\, g\rangle\langle n,\, g| + |n,\, r(l)\rangle\langle n, r(l)|)], \end{aligned} \tag{19}$$

where φ and ρ denote the steady state and the steady-state density matrix of the system driven from its upper (lower) side which is described by the Hamiltonian $\hat{H}_{\circlearrowleft}$ ($\hat{H}_{\circlearrowright}$), n denotes the intracavity photon number of the mode $\hat{a}_{\circlearrowleft}$ ($\hat{a}_{\circlearrowright}$), g and r (l) denote the atom in the ground and excited state. The Poisson distribution is defined as $\mathcal{P}(n) = (\langle\hat{n}_x\rangle^n/n!)\exp(-\langle\hat{n}_x\rangle)$. In Fig. 3(c-i), where driving comes from the resonator's upper side, single-photon probability is enhanced as $P(1) > \mathcal{P}(1)$, while m-photon ($m = 2,\ 3,\ 4$) probabilities are suppressed as $P(m) < \mathcal{P}(m)$ at $\Delta = -2\delta$. This consists with the case that the first photon blocks the entrance of a second photon, which indicates the enhancement of the single-photon probability and the suppression of multi-photon probabilities. In Fig. 3(c-ii), where driving comes from the lower side, single-photon probability is suppressed while multi-photon probabilities are enhanced at $\Delta = -2\delta$, i.e., $P(1) < \mathcal{P}(1)$ and $P(m) > \mathcal{P}(m)$. This deviation of the intracavity photon-number distribution $P(n)$ from $\mathcal{P}(n)$ clearly characterizes multi-photon tunneling and is in sharp contrast to that of the case when driving from the upper side.

Feasibility and Implementation. For experimental implementations, two laser beams are used to pump the ^{87}Rb atom into the ground state $|5S_{1/2},\, F = 1,\, m_{\mathrm{F}} = 0\rangle$. One of them is a linearly polarized beam tuned to the $|5S_{1/2},\, F = 2\rangle \leftrightarrow |5P_{3/2},\, F' = 2\rangle$ transition and it pumps the ^{87}Rb atom in the $|5S_{1/2},\, F = 2\rangle$ state to the $|5S_{1/2},\, F = 1\rangle$ state. It is called hyperfine pumping. The other is a linearly polarized beam tuned to the $|5S_{1/2},\, F = 1\rangle \leftrightarrow |5P_{3/2},\, F' = 1\rangle$ transition and it pumps the ^{87}Rb atom into the $|5S_{1/2},\, F = 1,\, m_{\mathrm{F}} = 0\rangle$ state. It is called the Zeeman pumping beam. The resonator has a 2.2-mm radius and a refractive index of $n = 3.48$. The transmission efficiency at the interface between WG1 (WG2) and the resonator is 99.9%, yielding a corresponding external decay rate $\kappa_{\mathrm{ex},\,1}$ ($\kappa_{\mathrm{ex},\,2}$) of about $2\pi \times 1\,\mathrm{MHz}$. The total decay rate of the CW (CCW) mode is $\kappa = \kappa_{\mathrm{ex},\,1} + \kappa_{\mathrm{ex},\,2}$. The resonator is approximately 0.63 μm wide and 0.63 μm thick, leading to a mode volume $V_{\mathrm{m}} \approx 5426\,\mu\mathrm{m}^3$. Correspondingly, the strength of the zero-point fluctuation of this mode is $|\mathbf{E}_0| = \sqrt{\frac{\hbar\omega_a}{2\epsilon_0 V_{\mathrm{m}}}} \approx 1.6 \times 10^3\,\mathrm{V/m}$, where ϵ_0 is the vacuum permittivity and $\omega_a/2\pi \approx 377.11\,\mathrm{THz}$ is the resonance frequency of the WGM resonator. The dipole moments of the atomic σ^+ and σ^- transitions $|5S_{1/2},\, F = 1,\, m_{\mathrm{F}} = 0\rangle \leftrightarrow |5P_{1/2},\, F' = 2,\, m_{\mathrm{F}'} = \pm 1\rangle$ are both $2|\mathbf{d}| = 2.5377 \times 10^{-29}\,\mathrm{C{\cdot}m}$. Therefore, the coupling strength between the Rb atom and the CW (CCW) mode is $g = \frac{\mathbf{d}\cdot\mathbf{E}_0}{\hbar} = 2\pi \times 30.88\,\mathrm{MHz}$.

In conclusion, we have proposed an integrable nonreciprocal quantum scheme with a microring resonator coupled to a light-controlled V-type atom. A circularly polarized control laser generates the FMF and thus induces the Zeeman splitting of atomic hyperfine sublevels. The countercirculating resonator modes couple to the splitting σ^+ and σ^- atomic transitions with red and blue detunings. This directional detuning induces the directional eigenspectra of the resonator-atom coupling system. Single-photon blockade emerges when driven from the one side and two-photon tunneling emerges when driven from the other side. A strong quantum nonreciprocity, with up to three orders of magnitude difference of $g^{(2)}(0)$ for opposite directions, is obtained. A deep PB with $g^{(2)}(0) \sim 0.2$ is shown simultaneously.

Our scheme provides a novel mechanism to achieve quantum nonreciprocity as presented in Refs. [30,31], without the requirement for mechanical rotation or real magnetic fields. This mechanism can be extended to various wavelength bands and different device platforms, such as traveling-wave resonators coupled with atom-like emitters. Moreover, our proposal promises an on-chip platform for high-quality unidirectional single-photon sources, which are crucial elements in quantum information processing and chiral quantum networks.

Acknowledgements. This work was supported by the National Natural Science Foundation of China (Grant Nos. 12305020 and 92365107), the National Key R&D Program of China (Grant No. 2019YFA0308700), the Program for Innovative Talents and Teams in Jiangsu (Grant No. JSSCTD202138), China Postdoctoral Science Foundation (Grant No. 2023M731613), and Jiangsu Funding Program for Excellent Postdoctoral Talent (Grant No. 2023ZB708).

References

[1] Asadchy V S, Mirmoosa M S, Díaz-Rubio A, Fan S, and Tretyakov S A 2020 *Proc. IEEE* **108** 1684
[2] Caloz C, Alù A, Tretyakov S, Sounas D, Achouri K, and Deck-Léger Z L 2018 *Phys. Rev. Appl.* **10** 047001
[3] Freiser M 1968 *IEEE Trans. Magn.* **4** 152
[4] Haider T 2017 *Int. J. Electromagnet. Appl.* **7** 17
[5] Zhang T T, Zhou W P, Li Z X, Tang Y T, Xu F, Wu H D, Zhang H, Tang J S, Ruan Y P, and Xia K Y 2024 *Chin. Phys. Lett.* **41** 044205
[6] Fan L, Wang J, Varghese L T, Shen H, Niu B, Xuan Y, Weiner A M, and Qi M 2012 *Science* **335** 447
[7] Peng B, Özdemir Ş K, Lei F C, Monifi F, Gianfreda M, Long G L, Fan S H, Nori F, Bender C M, and Yang L 2014 *Nat. Phys.* **10** 394
[8] Chang L, Jiang X, Hua S, Yang C, Wen J, Jiang L, Li G, Wang G, and Xiao M 2014 *Nat. Photon.* **8** 524
[9] Hua S, Wen J, Jiang X, Hua Q, Jiang L, and Xiao M 2016 *Nat. Commun.* **7** 13657
[10] Li C, Yu Q, Zhang Y, Xiao M, and Zhang Z 2023 *Laser Photon. Rev.* **17** 2200267
[11] Lin G, Zhang S, Hu Y, Niu Y, Gong J, and Gong S 2019 *Phys. Rev. Lett.* **123** 033902
[12] Kamal A, Clarke J, and Devoret M H 2011 *Nat. Phys.* **7** 311
[13] Del Bino L, Silver J M, Woodley M T M, Stebbings S L, Zhao X, and Del'Haye P 2018 *Optica* **5** 279
[14] Tang L, Tang J, Wu H, Zhang J, Xiao M, and Xia K 2021 *Photon. Res.* **9** 1218

[15] Pan R K, Tang L, Xia K, and Nori F 2022 *Chin. Phys. Lett.* **39** 124201
[16] Yu Z and Fan S 2009 *Nat. Photon.* **3** 91
[17] Lira H, Yu Z, Fan S, and Lipson M 2012 *Phys. Rev. Lett.* **109** 033901
[18] Sounas D L and Alù A 2017 *Nat. Photon.* **11** 774
[19] Estep N A, Sounas D L, Soric J, and Alù A 2014 *Nat. Phys.* **10** 923
[20] Kittlaus E A, Jones W M, Rakich P T, Otterstrom N T, Muller R E, and Rais-Zadeh M 2021 *Nat. Photon.* **15** 43
[21] Xia K, Nori F, and Xiao M 2018 *Phys. Rev. Lett.* **121** 203602
[22] Zhang S, Hu Y, Lin G, Niu Y, Xia K, Gong J, and Gong S 2018 *Nat. Photon.* **12** 744
[23] Dong M X, Xia K Y, Zhang W H, Yu Y C, Ye Y H, Li E Z, Zeng L, Ding D S, Shi B S, Guo G C, and Nori F 2021 *Sci. Adv.* **7** eabe8924
[24] Liang C, Liu B, Xu A N, Wen X, Lu C, Xia K, Tey M K, Liu Y C, and You L 2020 *Phys. Rev. Lett.* **125** 123901
[25] Manipatruni S, Robinson J T, and Lipson M 2009 *Phys. Rev. Lett.* **102** 213903
[26] Shen Z, Zhang Y L, Chen Y, Zou C L, Xiao Y F, Zou X B, Sun F W, Guo G C, and Dong C H 2016 *Nat. Photon.* **10** 657
[27] Shen Z, Zhang Y L, Chen Y, Sun F W, Zou X B, Guo G C, Zou C L, and Dong C H 2018 *Nat. Commun.* **9** 1797
[28] Ruesink F, Miri M A, Alù A, and Verhagen E 2016 *Nat. Commun.* **7** 13662
[29] Fang K, Luo J, Metelmann A, Matheny M H, Marquardt F, Clerk A A, and Painter O 2017 *Nat. Phys.* **13** 465
[30] Maayani S, Dahan R, Kligerman Y, Moses E, Hassan A U, Jing H, Nori F, Christodoulides D N, and Carmon T 2018 *Nature* **558** 569
[31] Huang R, Miranowicz A, Liao J Q, Nori F, and Jing H 2018 *Phys. Rev. Lett.* **121** 153601
[32] Xue W S, Shen H Z, and Yi X X 2020 *Opt. Lett.* **45** 4424
[33] Xu X, Zhao Y, Wang H, Jing H, and Chen A 2020 *Photon. Res.* **8** 143
[34] Li B, Huang R, Xu X, Miranowicz A, and Jing H 2019 *Photon. Res.* **7** 630
[35] Shen H Z, Wang Q, Wang J, and Yi X X 2020 *Phys. Rev. A* **101** 013826
[36] Xiang Y, Zuo Y, Xu X W, Huang R, and Jing H 2023 *Phys. Rev. A* **108** 043702
[37] Jiao Y F, Zhang S D, Zhang Y L, Miranowicz A, Kuang L M, and Jing H 2020 *Phys. Rev. Lett.* **125** 143605
[38] Horsley S A R, Wu J H, Artoni M, and La Rocca G C 2013 *Phys. Rev. Lett.* **110** 223602
[39] Wang D W, Zhou H T, Guo M J, Zhang J X, Evers J, and Zhu S Y 2013 *Phys. Rev. Lett.* **110** 093901
[40] Wu J H, Artoni M, and La Rocca G C 2014 *Phys. Rev. Lett.* **113** 123004
[41] Lodahl P, Mahmoodian S, Stobbe S, Rauschenbeutel A, Schneeweiss P, Volz J, Pichler H, and Zoller P 2017 *Nature* **541** 473
[42] Scheucher M, Hilico A, Will E, Volz J, and Rauschenbeutel A 2016 *Science* **354** 1577
[43] Shomroni I, Rosenblum S, Lovsky Y, Bechler O, Guendelman G, and Dayan B 2014 *Science* **345** 903
[44] Söllner I, Mahmoodian S, Hansen S L, Midolo L, Javadi A, Kiršanskė G, Pregnolato T, El-Ella H, Lee E H, Song J D, Stobbe S, and Lodahl P 2015 *Nat. Nanotechnol.* **10** 775
[45] Xia K, Lu G, Lin G, Cheng Y, Niu Y, Gong S, and Twamley J 2014 *Phys. Rev. A* **90** 043802
[46] Tang L, Tang J, Zhang W, Lu G, Zhang H, Zhang Y, Xia K, and Xiao M 2019 *Phys. Rev. A* **99** 043833
[47] Hu X X, Wang Z B, Zhang P, Chen G J, Zhang Y L, Li G, Zou X B, Zhang T, Tang H X, Dong C H, Guo G C, and Zou C L 2021 *Nat. Commun.* **12** 2389
[48] Yang P, Li M, Han X, He H, Li G, Zou C L, Zhang P, Qian Y, and Zhang T 2023 *Laser Photon. Rev.* **17** 2200574
[49] Tang J S, Nie W, Tang L, Chen M, Su X, Lu Y, Nori F, and Xia K 2022 *Phys. Rev. Lett.* **128** 203602
[50] Malz D, Tóth L D, Bernier N R, Feofanov A K, Kippenberg T J, and Nunnenkamp A 2018 *Phys. Rev. Lett.* **120** 023601
[51] Abdo B, Sliwa K, Shankar S, Hatridge M, Frunzio L, Schoelkopf R, and Devoret M 2014 *Phys. Rev. Lett.* **112** 167701
[52] Metelmann A and Clerk A A 2015 *Phys. Rev. X* **5** 021025
[53] Liu D W, Li Z H, Chao S L, Wu Y, and Si L G 2024 *Sci. China Phys. Mech.* **67** 260313
[54] Birnbaum K M, Boca A, Miller R, Boozer A D, Northup T E, and Kimble H J 2005 *Nature* **436** 87
[55] Dayan B, Parkins A S, Aoki T, Ostby E P, Vahala K J, and Kimble H J 2008 *Science* **319** 1062
[56] Hamsen C, Tolazzi K N, Wilk T, and Rempe G 2018 *Nat. Phys.* **14** 885
[57] Faraon A, Fushman I, Englund D, Stoltz N, Petroff P, and Vučković J 2008 *Nat. Phys.* **4** 859
[58] Tang J, Tang L, Wu H, Wu Y, Sun H, Zhang H, Li T, Lu Y, Xiao M, and Xia K 2021 *Phys. Rev. Appl.* **15** 064020
[59] Chen M, Tang J, Tang L, Wu H, and Xia K 2022 *Phys. Rev. Res.* **4** 033083
[60] Lang C, Bozyigit D, Eichler C, Steffen L, Fink J M, Abdumalikov A A, Baur M, Filipp S, da Silva M P, Blais A, and Wallraff A 2011 *Phys. Rev. Lett.* **106** 243601
[61] Liu Y X, Xu X W, Miranowicz A, and Nori F 2014 *Phys. Rev. A* **89** 043818
[62] Hoffman A J, Srinivasan S J, Schmidt S, Spietz L, Aumentado J, Türeci H E, and Houck A A 2011 *Phys. Rev. Lett.* **107** 053602
[63] Tang J, Wu Y, Wang Z, Sun H, Tang L, Zhang H, Li T, Lu Y, Xiao M, and Xia K 2020 *Phys. Rev. A* **101** 053802
[64] Peyronel T, Firstenberg O, Liang Q Y, Hofferberth S, Gorshkov A V, Pohl T, Lukin M D, and Vuletić V 2012 *Nature* **488** 57
[65] Firstenberg O, Peyronel T, Liang Q Y, Gorshkov A V, Lukin M D, and Vuletić V 2013 *Nature* **502** 71
[66] Rabl P 2011 *Phys. Rev. Lett.* **107** 063601
[67] Nunnenkamp A, Børkje K, and Girvin S M 2011 *Phys. Rev. Lett.* **107** 063602
[68] Liao J Q and Nori F 2013 *Phys. Rev. A* **88** 023853
[69] Imamoğlu A, Schmidt H, Woods G, and Deutsch M 1997 *Phys. Rev. Lett.* **79** 1467
[70] Werner M J and Imamoğlu A 1999 *Phys. Rev. A* **61** 011801
[71] Miranowicz A, Paprzycka M, Liu Y X, Bajer J, and Nori F 2013 *Phys. Rev. A* **87** 023809
[72] Su X, Tang J S, and Xia K 2022 *Phys. Rev. A* **106** 063707
[73] Huang R, Özdemir Ş K, Liao J Q, Minganti F, Kuang L M, Nori F, and Jing H 2022 *Laser Photon. Rev.* **16** 2100430
[74] Zuo Y, Huang R, Kuang L M, Xu X W, and Jing H 2022 *Phys. Rev. A* **106** 043715
[75] Cohen-Tannoudji C and Dupont-Roc J 1972 *Phys. Rev. A* **5** 968
[76] Le Kien F, Schneeweiss P, and Rauschenbeutel A 2013 *Eur. Phys. J. D* **67** 92
[77] Rosenbusch P, Ghezali S, Dzuba V A, Flambaum V V, Beloy K, and Derevianko A 2009 *Phys. Rev. A* **79** 013404
[78] Park C Y, Noh H, Lee C M, and Cho D 2001 *Phys. Rev. A* **63** 032512
[79] Leszczyński A, Mazelanik M, Lipka M, Parniak M, Dąbrowski M, and Wasilewski W 2018 *Opt. Lett.* **43** 1147
[80] Junge C, O'Shea D, Volz J, and Rauschenbeutel A 2013 *Phys. Rev. Lett.* **110** 213604
[81] Shao Z, Zhu J, Chen Y, Zhang Y, and Yu S 2018 *Nat. Commun.* **9** 926